Thermal Effects in Monolithically Integrated Tunable Laser Transmitters

Peter Kozodoy, Tim Strand, Yuliya Akulova, Greg Fish, Clint Schow, Ping Koh
Agility Communications, Inc.
475 Pine Avenue
Santa Barbara CA 93117

Zhixi Bian, James Christofferson, Ali Shakouri
Baskin School of Engineering
University of California
Santa Cruz CA 95064

Abstract

We investigate thermal effects in widely-tunable laser transmitters based on an integrated single chip design. The chip contains a Sampled-Grating Distributed Bragg Reflector (SG-DBR) laser monolithically integrated with a semiconductor optical amplifier (SOA) and an electroabsorption modulator (EAM). The thermal impedance of the ridge structure is evaluated through simulation and experiment, and thermal crosstalk between sections is examined. Heating of the mirrors by neighboring sections is found to result in unintentional offsets in wavelength tuning. Thermal effects in the electroabsorption modulator are examined in depth. A positive feedback mechanism causes local temperature rise at the modulator input, with the potential to trigger catastrophic thermal runaway. A self-consistent finite-element model is developed to simulate the EAM temperature profile and device performance. This model is used to optimize the device, resulting in integrated EAMs that achieve a dissipated power limit in excess of 300 mW.

Keywords

Integrated optoelectronics, tunable laser, semiconductor laser, thermal crosstalk, thermal impedance, semiconductor optical amplifier, electroabsorption modulator, thermal runaway

1. Introduction

Photonic integrated circuits offer significant performance advantages over discrete devices, adding flexibility and functionality while reducing final system cost and size. Commercial development of these devices has required careful engineering to enable integration using a common layer structure and processing sequence. An additional engineering constraint is the strong thermal sensitivity of these structures. It has long been recognized that optoelectronic devices are particularly sensitive to thermal effects, as numerous material parameters are strongly affected by internal heating. This sensitivity is compounded in integrated structures, where thermal cross-talk between elements must be considered.[1-4] Furthermore, integrated devices designed for wide tunability may be inherently more sensitive to index shifts caused by small thermal changes.[5]

This paper focuses on thermal effects in a monolithic widely-tunable sampled grating distributed Bragg reflector (SG-DBR) laser source with an integrated semiconductor optical amplifier (SOA) and electroabsorption modulator (EAM). The SG-DBR laser design produces a device with an emission wavelength that can be tuned within a 40 nm range, covering the entire C-band from 1528 nm to 1568 nm.

Modern dense wavelength-division-multiplexing (DWDM) optical communication systems can employ more than 100 channels over a single fiber. Most of these systems operate in the C-band, with channel spacing of 25 or 50 GHz. Typically, separate fixed-wavelength lasers are made and individually selected for a specific wavelength in a DWDM system. Thus, for an 80 channel systems, 80 different lasers are required, each with a different wavelength. Widely tunable lasers, in contrast, are capable of generating every optical channel in the entire C-band. Thus, one tunable laser can replace any fixed wavelength laser in a DWDM system simply by setting it to the desired wavelength. Furthermore, the next generation of re-configurable optical networks [6,7] will require tunable lasers as light sources that can switch operating wavelength on the fly. Re-configurable networks offer a higher degree of flexibility for capacity allocation. This is expected to become an increasingly important feature, especially in the metro space where traffic patterns are more fluid.

The device described in this paper has been designed for such metro applications. The SG-DBR laser design provides tunability across the entire C-band with very fast switching times. The integrated SOA boosts the power output of the chip, and provides wavelength independent power leveling. Also integrated on the chip is an electroabsorption modulator. This device modulates the output power of the chip according to an electrical data input stream, allowing the chip to operate as an integrated laser transmitter rather than a CW source requiring external modulation. This monolithic integration scheme reduces power consumption by eliminating the optical coupling loss associated with an external modulator. Monolithic integration also reduces the size and cost of the final product.

These integrated devices operate at 2.5 Gb/s and are now commercially available. The chips combine light generation, wavelength tuning, light amplification and leveling, and light modulation in a single device. They are an example of the highest level of integration in the field of optoelectronics. Due to this high level of integration, thermal effects are a

Due to this high level of integration, thermal effects are a primary concern in the design of these devices. Two areas of particular interest are addressed in this paper: the effect of thermal cross-talk on mirror tuning, and thermal optimization of the EAM section.

2. Device Description

The integrated structure, shown in figure 1, is produced on an epitaxial growth that includes an InGaAsP waveguide layer common to all sections, topped by a multi-quantum well active region for light emission. The active region is selectively etched away in all areas except the gain and amplifier sections. Holographically defined Bragg gratings are etched into the waveguide layer in the front and back mirror sections. Additional periodicity is imposed on the gratings through "sampling" (periodic blanking of the grating). Device fabrication concludes with regrowth of a p-InP cladding layer, formation of a ridge waveguide that connects all sections, and the deposition of a dielectric cladding layer and metal contacts.

Sampling the grating structure introduces additional periodicity to the DBRs, and transforms the reflectivity spectra of the mirrors into a comb of reflectivity peaks centered on the Bragg wavelength. The front and back mirrors of the laser are sampled at different periods such that only one of their multiple reflection peaks coincides at a time. This creates a Vernier effect that enables a wide wavelength tuning range. Tuning is accomplished through current injection into the mirror sections, altering the refractive index and causing adjacent reflectivity maxima to come into alignment, thereby shifting the lasing wavelength a large amount for a small index change. This is illustrated in figure 2. Continuous tuning between the reflectivity maxima is obtained by tuning both mirrors simultaneously. Biasing of the phase section fine-tunes the effective Fabry-Perot cavity mode into alignment with the maximum reflectivity of the mirrors. The tuning range of a SG-DBR laser is defined by the repeat mode spacing and can be designed to exceed the tuning range of a conventional DBR laser by a factor of ten. Optimization of the device for C-band operation is accomplished by alignment of the gain spectra and Bragg wavelength of the
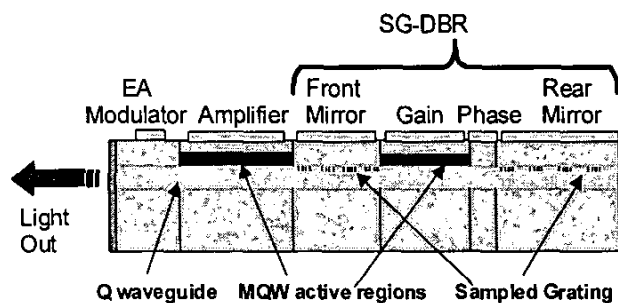
holographically defined grating within the band.

The integrated SOA compensates on-state modulator loss and cavity losses caused by free carrier absorption in the tuning sections, and allows wavelength independent power leveling. It can also be used as a variable optical attenuator (VOA). The electroabsorption modulator operates through the Franz-Keldysh effect in the bulk waveguide material. This effect describes the absorption of sub-bandgap light through a tunneling mechanism when an electric field is applied. The waveguide composition has been optimized to achieve high tuning efficiency for the laser and a target extinction ratio over the required wide spectral bandwidth for the modulator. The final device is placed on an AlN carrier and mounted into a cooled butterfly module with a coplanar RF input. A multichannel wavelength locker is integrated into the package. This package is then integrated into a compact transmitter assembly along with electronics to provide the DC current sources, modulator driver, and device control loops.
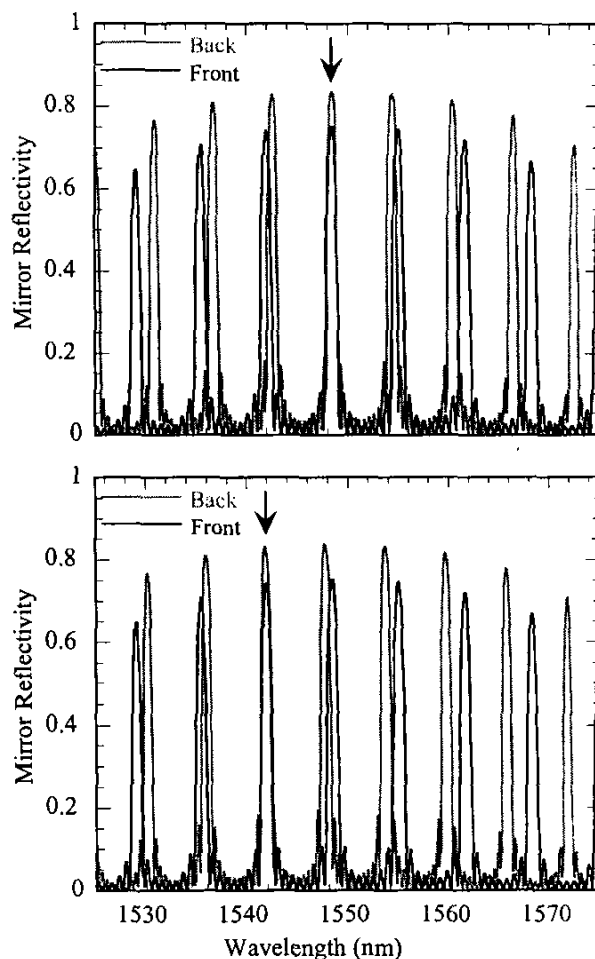

Figure 1: Schematic diagram of the chip with integrated tunable SG-DBR laser, semiconductor optical amplifier, and EA modulator.

Figure 2: Overlaid mirror reflectivity spectra calculated for two different back mirror current levels. A small change in back mirror index results in a large shift in lasing wavelength (Vernier effect).

In RF operation, the device produces time-averaged powers in excess of 5 dBm, RF extinction ratios greater than 10 dB, and error-free transmission at 2.5 Gb/s over 350 km of standard single mode fiber, across a 40 nm tuning range. In CW operation, the module meets all long-haul system requirements for externally modulated laser sources: stability, power (> 10 mW), RIN (< -140 dB/Hz), and linewidth (< 2 MHz) over 90 50-GHz spaced ITU channels. Further details on device performance are provided in reference [8].

3. Thermal cross-talk

Heat spreading between sections was calculated using a two-dimensional finite element model that considered the entire chip situated on the AlN carrier. Figure 3(a) shows the calculated temperature profile resulting from each of the sections independently dissipating one watt. Heating any one section produces a measurable temperature rise in all other sections. Under standard CW operating conditions, with the modulator unbiased, the calculated temperature profile is shown in figure 3(b). It is clear that the temperature profile of the passive sections is dominated not by self-heating but by cross-talk heating from the neighboring active sections, which are driven at a much higher current density. This can have an important effect on device operation, as the temperature rise
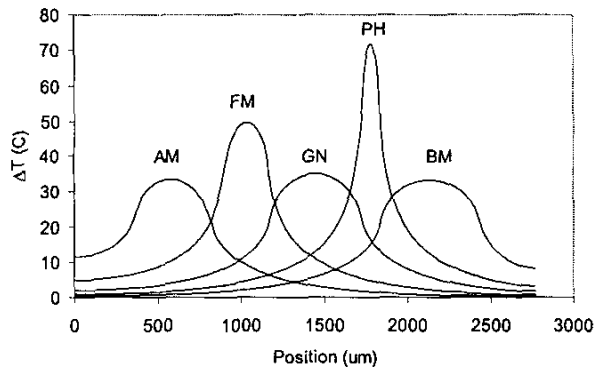

Figure 3(a): Calculated longitudinal temperature profiles in chip, resulting from individual sections dissipating one watt. Heat from each section is measurable in all other sections.
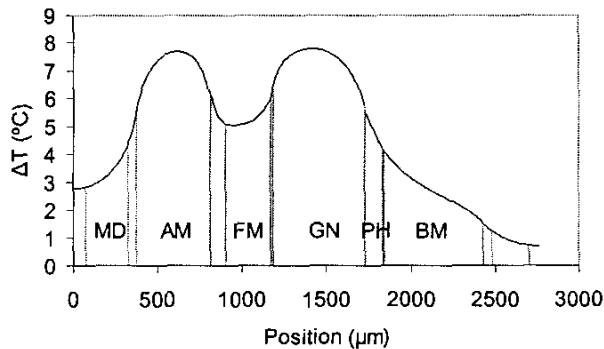

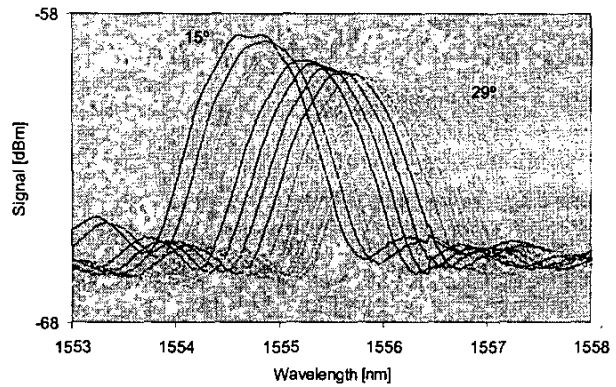Figure 3(b): Modeled longitudinal temperature profile under typical operating conditions.

Figure 4: Front mirror peaks observed by driving the amplifier section at a fixed current and varying the stage temperature from 15 C to 29 C in increments of 1 C.

will produce an index shift and, therefore, affect the tuning properties of the device.

An experiment was performed in order to validate the calculated cross-talk parameters. When driving the amplifier section and monitoring the optical output spectrum, the broad gain peak of the amplifier appears overlaid with the front mirror reflection peaks. The position of these peaks is determined by temperature (figure 4), so a CW measurement can be used to determine the heating of the front mirror by the amplifier section. By holding the stage temperature fixed while varying the amplifier current, a cross-talk thermal impedance of 9.8 K/W was measured. This compares very well with the calculated value of 9.4 K/W, obtained from a two-dimensional finite-element simulation using the known thermal impedance values of the constituent materials.

These results also provide a quantitative measure of mirror tuning as a function of temperature. Figure 4 indicates individual mirror tuning of > 100 pm/°C. Under normal laser operation, this tuning will be greatly amplified by the Vernier effect, so that significant wavelength changes will result from
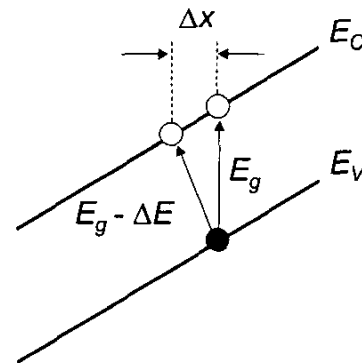

Figure 5: Schematic of photon absorption under high electric field. Sub-bandgap light is absorbed through a tunneling mechanism. After reference [11].
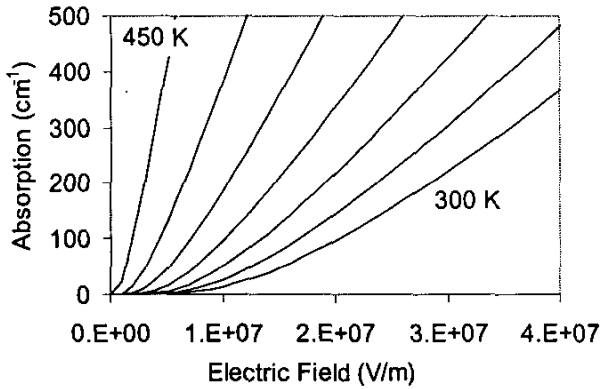
Figure 6: Waveguide absorption calculated as a function of electric field. The temperature is varied from 300K to 450K in steps of 25K. Input wavelength is 1548 nm.

any temperature difference between the two mirror sections. Indeed, intentional use of such thermal tuning in SGDBRs has been demonstrated using integrated micro-heaters; Ishii et. al. report a 40 nm tuning range achieved with 50°C temperature tuning.[9] This technique produces widely-tunable lasers with low linewidth, but switching times are very slow due to the long thermal constants. In the present devices, fast tuning is accomplished through carrier injection, and so this thermal tuning is undesirable. Care must be taken to calibrate out the thermal effects by testing the tuning properties of each device at all target power levels. Calibrated tuning currents, stored in the module firmware, are used to select wavelength channels during operation.

4. Electroabsorption Modulator Optimization

The electroabsorption modulator will experience the strongest thermal effects of any section in the integrated device. This is due to a positive feedback cycle that is created: as incident light is absorbed in the modulator, Joule heating occurs due to the applied voltage and the photocurrent that is produced. This heating causes a local reduction in
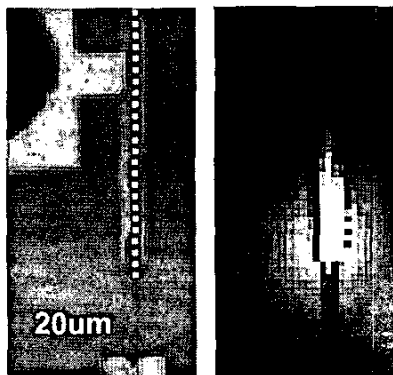

Figure 7: Optical (left) and thermoreflectance (right) image of an electroabsorption modulator biased at –2.7 V. The dotted line along the ridge indicates the position of the line scan used in figure 6.

bandgap, which in turn increases absorption, causing additional heating. This effect will be strongest at the front of the device, where the optical power is high.

Two formulae are needed in order to calculate local absorption as a function of electric field and local temperature. The Franz-Keldysh effect describes the absorption of sub-bandgap light as a function of electric field and photon energy.[10] This mechanism is shown schematically in figure 5. Thermal shrinkage of the bandgap will cause this absorption to increase by bringing the optical energy closer to the bandgap, thus increasing the tunneling probability. The bandgap variation with temperature is described empirically by the Varshni equations.[12] Combining these formulae, absorption characteristics can be calculated for the InGaAsP waveguide used in this device. The results of this calculation are presented in figure 6 for incident light at a wavelength of 1548 nm.

The potential for strong positive feedback is clear from figure 6, which shows the optical absorption to be highly sensitive to temperature changes. This feedback cycle can turn catastrophic at sufficiently high input power levels or large bias values. Under these conditions, the interaction between absorption and temperature will lead to increasing heat localization at the input of the modulator, triggering thermal run-away and causing severe device damage. The local self-heating phenomenon is also significant, however, at the lower values of input power and device bias typically used during operation. Indeed, we found it impossible to match device performance to calculated models without taking this effect into account.
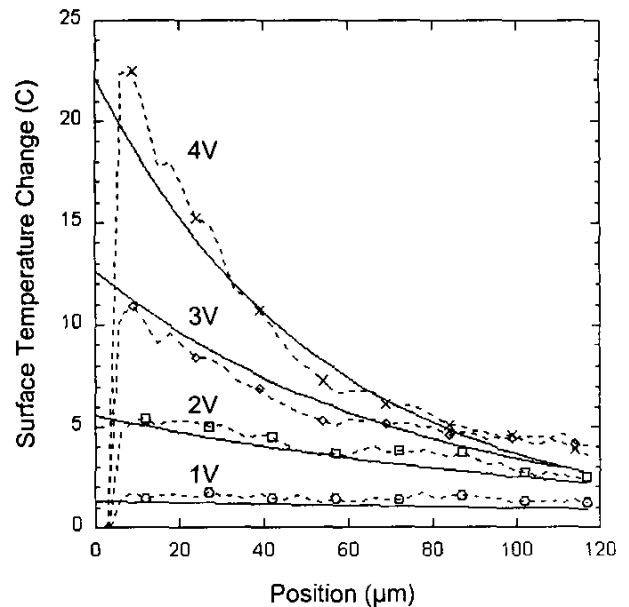

Figure 8: Surface temperature rise along the ridge: thermoreflectance measurement (dashed line) and model (solid line). Input power is ~ 6 mW, and operating wavelength is 1548 nm.
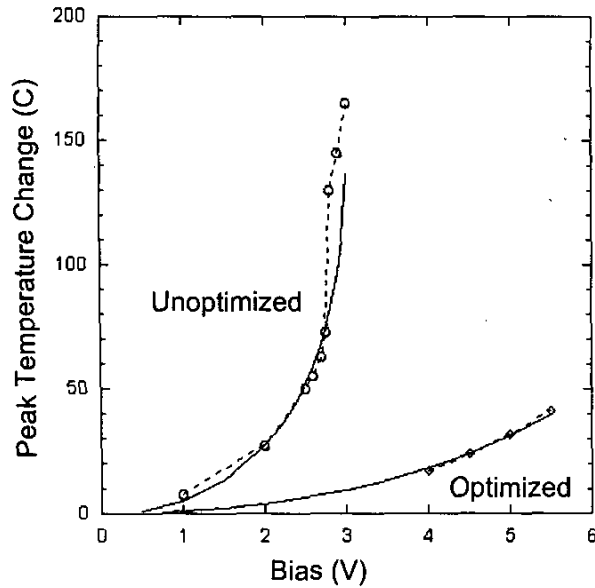
Figure 9: Maximum temperature as a function of modulator bias: thermoreflectance measurement (dashed line) and model (solid line). The input power is around 35 mW, and operating wavelength is 1548 nm.

Previous published work has investigated EAM breakdown [13] and shown evidence of heating non-uniformity.[14] In this work, we present a detailed analysis of temperature effects in EAM structures, examining two modulator designs both experimentally and theoretically. The composition and thickness of the intrinsic waveguide layer was kept constant, but two different thermal designs were employed: an unoptimized design and an optimized one. Experimental measurements were performed using a thermal
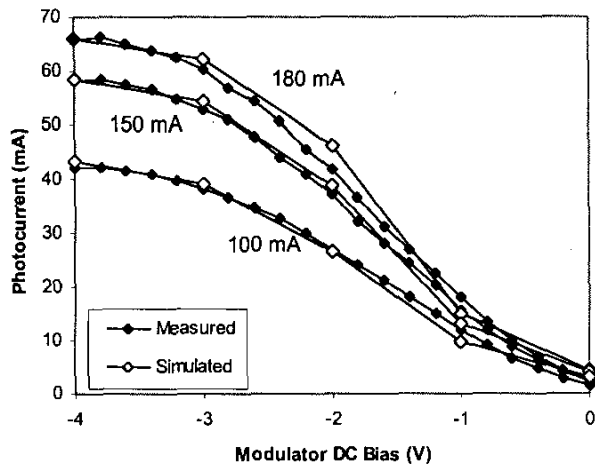
imaging technique based on thermoreflectance. This thermal imaging system has achieved submicron spatial resolution and < 0.1°C temperature resolution; details of the measurement technique and initial results are described in reference [15]. Figure 7 shows images of the EAM device under operation; significant heating localized at the front of the modulator is clearly evident.

A finite-element thermal model was developed for comparison to the experimental results. This one-dimensional model calculates optical power absorption, local photocurrent, and local temperature self-consistently using the Varshni equations for thermal bandgap shrinkage.[12] Thermal impedance values are calculated from a detailed analysis of the ridge cross-section. Figure 8 shows measured and calculated thermal profiles at low input power, along the longitudinal axis of the unoptimized EAM. Excellent agreement is obtained between the calculated and measured distributions. Figure 9 compares the bias dependence of the peak temperature under high optical input power (~ 35 mW at 1548 nm) for the two different modulator designs. The unoptimized design clearly exhibits thermal runaway at ~ 2.75 V, with very high surface temperatures indicated. In contrast, the optimized structure, using the same epitaxial layer structure, exhibits much lower heating and can be operated to higher voltages without triggering thermal runaway. These optimized devices consistently achieve damage-free operation at a DC bias of 5 V and well over 60 mA photocurrent (total electrical power in excess of 300 mW).

The self-consistent finite element model has been extended in order to calculate the electrical and optical performance of the optimized EAMs, under both DC and RF modulation. Figure 10 shows calculated and measured values of device photocurrent as a function of DC bias at three different amplifier current levels.
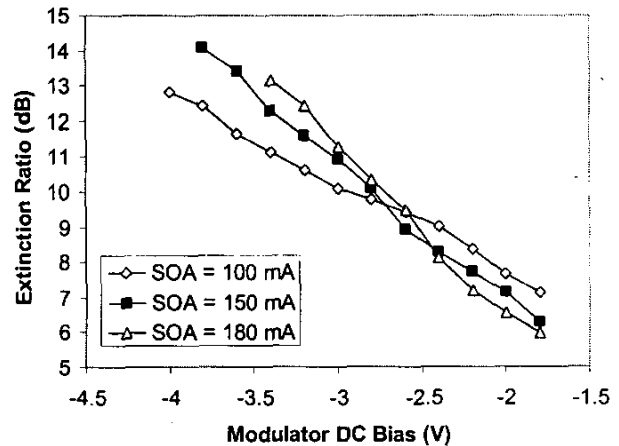

Figure 10: Device photocurrent as a function of modulator DC bias, for three different amplifier currents: measured values (solid symbols) and model (open symbols). Operating wavelength is 1545 nm.

Figure 11: Measured RF extinction ratio as a function of modulator DC bias. The RF driver voltage is kept constant at 3.4V peak-to-peak, and modulation rate is 2.5 Gb/sec. Operating wavelength is 1545 nm. SOA current is varied.

Extending this model to the RF domain requires developing a model for high frequency voltage transfer from the driver to the EAM. The measured RF extinction ratio plotted in figure 11 illustrates the importance of this parameter. In a simple application of the EAM theory, one would expect the extinction ratio to be independent of the optical input power (controlled in this case by the SOA current). Instead, we observe two regimes of behavior: at low DC voltage, a higher extinction ratio is achieved at low optical input power, while at high DC voltage the opposite is true. The high voltage effect is a direct result of the heating phenomena that have already been discussed. The high photocurrent that is generated under large optical input power causes a substantial temperature rise; this increases the total light absorption, raising the extinction ratio.

The variation in extinction ratio at low DC bias, however, results from a different phenomenon: variation in the quality of the RF match between the EAM and the driver circuit. When the dynamic resistance of the EAM is low (i.e. the photocurrent varies strongly with applied bias), significant voltage reflections occur and the full driver voltage is not transferred to the EAM. Higher optical input power leads to a lower dynamic resistance, causing a degraded extinction ratio as less of the RF voltage is delivered to the modulator. It is important to include both of these effects in the finite element model in order to achieve a good fit to experimentally measured data.

In order to model the RF voltage reflections, dynamic resistance values were extracted from the simulated DC I-V
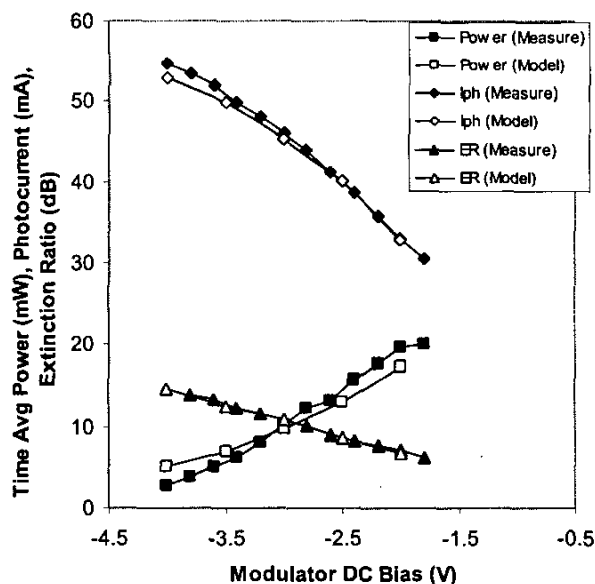

Figure 12: Device output power, photocurrent, and extinction ratio under RF operation: measured values (solid symbols) and model (open symbols). The DC bias is varied and the peak-to-peak RF driver bias is 3.4 V, with a modulation rate of 2.5 Gb/s. Operating wavelength is 1545 nm.

characteristics shown in figure 10, and these were used in an analysis of the RF matching network. The RF voltage transfer efficiency was calculated to lie between 65% and 100% of the driver voltage, depending on the DC bias point of the EAM and the input power level.

In modeling RF performance, the on-state and off-state voltage conditions were simulated independently, using time-averaged absorption to calculate the thermal profile. The RF simulations were performed at a range of DC bias values, using a fixed RF voltage (at the driver) of 3.4 V peak-to-peak. The input power was 49 mW (based on experimental measurements) and the operating wavelength was 1545 nm. The calculated values of output power, photocurrent, and extinction ratio are displayed in figure 12, along with experimental data obtained under the same operating conditions. The excellent agreement between measured and predicted device performance is further validation of this thermal model.

5. Conclusion

Thermal effects play an important role in the performance of widely-tunable SG-DBR lasers with integrated SOA and EAM sections. Strong effects include thermal crosstalk between the various sections, and thermal runaway effects in the electroabsorption modulator. In both cases, finite element models have successfully reproduced experimental data, and proved useful in optimizing the thermal performance of the device. The electroabsorption modulator has been examined in particular detail, as it experiences the most extreme temperatures in the chip. A self-consistent electrical, optical, and thermal finite-element model has been developed that successfully models the device performance. This model has been used to optimize the device, resulting in integrated EAMs that achieve a dissipated power limit in excess of 300 mW.

References

1. Y.H. Lo, T.P. Lee, "Very high speed OEIC transmitters for future optical transmission systems and optical networks," Intl J. High Speed Electronics, Vol. 2, pp. 21-44, 1991.

2. T. Wipiejewski, D.B. Young, B.J. Thibeault, L.A. Coldren, "Thermal crosstalk in 4*4 vertical-cavity surface-emitting laser arrays," IEEE Photonics Tech. Lett., Vol. 8, pp. 980-982, 1996.

3. B. Klepser, H. Hillmer, "Investigations of thermal crosstalk in laser arrays for WDM applications," J. Lightwave Technology, Vol. 16, pp. 1888-1894, 1998.

4. Chia-Chien Lin, Meng-Chyi Wu, Hung-Huei Liao, Wei-Han Wang, "Highly uniform operation of high-performance 1.3- mm AlGaInAs-InP monolithic laser arrays," IEEE J. Quantum Electronics, Vol. 36, pp. 590-597, 2000.

5. H. Okamoto, H. Yasaka, K. Sato, Y. Yoshikuni, K. Oe, K. Kishi, Y. Kondo, M. Yamamoto, "A wavelength-tunable duplex integrated light source for fast wavelength switching," J. Lightwave Tech., Vol. 14, pp. 1033-1041, 1996.

6. D. Arent, A. Martin, "Third-generation DWDM networks near reality," Lightwave by PennWell Corp., Vol. 18, No. 3, 2001.

7. R. Dhar, M. Lowry, "Tunable lasers create dynamic networking capabilities," WDM Solutions, pp. 83-88, Vol. 3, No. 9, 2001.

8. Y.A. Akulova, G.A. Fish, P.C. Koh, C. Schow, P. Kozodoy, A. Dahl, S. Nakagawa, M. Larson, M. Mack, T. Strand, C. Coldren, E. Hegblom, S. Penniman, T. Wipiejewski, L.A. Coldren, "Widely-Tunable Electroabsorption-Modulated Sampled Grating DBR Laser Transmitter," IEEE J. Select. Topics Quantum Electronics, Vol. 8, pp. 1349-1357, 2002.

9. H. Ishii, F. Kano, Y. Tohmori, Y. Kondo, T. Tamamura, Y. Yoshikuni, "Narrow Spectral Linewidth Under Wavelength Tuning in Thermally Tunable Super-Structure-Grating (SSG) DBR Lasers," IEEE J. Select. Topics Quantum Electronics, Vol. 1, pp. 401-407, 1995.

10. K. Wakita, Semiconductor Optical Modulators, Kluwer Academic Publishers (Boston, 1998), pp. 79-91.

11. L. Coldren, S. Corzine, Diode Lasers and Photonic Integrated Circuits, John Wiley and Sons (New York, 1995), p. 357.

12. H. Temkin, V.G. Keramidas, M.A. Pollack, and W.R. Wagner, "Temperature dependence of photoluminescence of n-InGaAsP," J. Appl. Phys., Vol. 52, p. 1574, 1981.

13. H. Tanaka, M. Horita, Y. Matsushima, Y. Takahashi, "Temperature Dependence and Input Optical Power Tolerance of an InGaAsP Electroabsorption Modulator Module," Optical and Quantum Electronics, Vol. 28, pp. 605-612, 1996.

14. M. Allard, R.A. Masut, M. Boudreau, "Temperature Determination in Optoelectronic Waveguide Modulators," J. Lightwave Technology, Vol. 18, pp. 813-818, 2000.

15. Z. Bian, J. Christofferson, A. Shakouri, P. Kozodoy, "High-Power Operation of Electroabsorption Modulators," Appl. Phys. Lett., Vol. 83, pp. 3605-3607, 2003.